Modeling Furanose Ring Dynamics in DNA

Gary A. Meints, Torgny Karlsson, and Gary P. Drobny*

Contribution from the Departments of Chemistry and Physics, University of Washington, Box 351700, Seattle, Washington 98195

Received March 19, 2001. Revised Manuscript Received June 19, 2001

Abstract: Determination of the conformational flexibility of the furanose ring is of vital importance in understanding the structure of DNA. In this work we have applied a model of furanose ring motion to the analysis of deuterium line shape data obtained from sugar rings in solid hydrated DNA. The model describes the angular trajectories of the atoms in the furanose ring in terms of pseudorotation puckering amplitude (q) and the pseudorotation puckering phase φ. Fixing q, the motion is thus treated as Brownian diffusion through an angular-dependent potential $U(\varphi)$. We have simulated numerous line shapes varying the adjustable parameters, including the diffusion coefficient D, pseudorotation puckering amplitude q, and the form of the potential $U(\varphi)$. We have used several forms of the potential, including equal double-well potentials, unequal double-well potentials, and a potential truncated to "second order" in the Fourier series. To date, we have obtained best simulations for both equilibrium and nonequilibrium (partially relaxed) solid-state deuterium NMR line shapes for the sample [2″-^{2}H]-2′-deoxycytidine at the position C3 (underlined) in the DNA sequence [d(CGCGAATTCGCG)]$_2$, using a double-well potential with an equal barrier height of $U_0 = 5.5k_BT$ (∼3.3 kcal/mol), a puckering amplitude of $q = 0.4$ Å, and a diffusion coefficient characterizing the underlying stochastic jump rate $D = 9.9 \times 10^8$ Hz. Then the rate of flux for the C−D bond over the barrier, i.e., the escape velocity or the overall rate of puckering between modes, was found to be 0.7×10^7 Hz.

Introduction

The furanose ring plays a pivotal role in DNA structure. In general, A-form DNA exhibits a C3′-endo configuration (see Figure 1b), and B-form DNA exhibits C2′-endo configuration (see Figure 1c),[1] and therefore the 2′-deoxyribose ring must have some degree of inherent conformational flexibility. Because the furanose ring may act as a buffer between the structurally labile phosphodiester backbone and the rigidly stacked base pairs, determination and quantification of the conformational flexibility of the furanose ring is of vital importance in understanding the structure of DNA.

X-ray crystallography and solution NMR have both contributed high-resolution structures of DNA, but neither technique has conclusively addressed the question of the conformational flexibility of the furanose sugars. Due to steric hindrance and ring strain, the five-membered furanose ring must be nonplanar, and conformational changes are accomplished by changes in the dihedral bond angles of the furanose ring. Due to the limited resolution of X-ray structures, conformational motions of the furanose ring would have to be directly deduced from motions of all the heavy atoms within the sugar, where whole amplitudes are small and on the order of <0.5 Å, or indirectly from correlation to the delta torsion angle.[2]

To determine dynamic amplitudes, crystallographic data are usually analyzed in terms of rigid body models, in which the constituent atoms of the furanose ring are assumed to move as a unit, as is the coupled base and its Watson−Crick pair partner.[3,4] Such methods are very informative of amplitudes of motion around assumed motional axes.

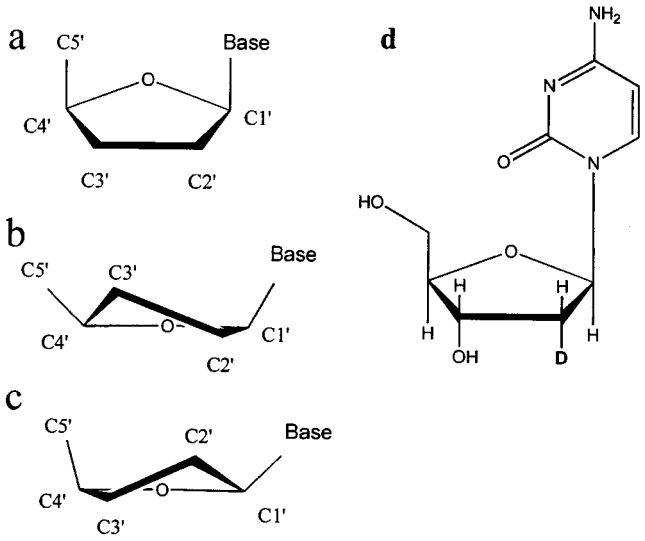

Figure 1. (a) Nomenclature for the carbon positions within a deoxyribose ring. (b) Schematic of C3′-endo conformation. (c) Schematic of C2′-endo conformation. (d) [2″-^{2}H]-2′-Deoxycytidine nucleoside used in this study.

Solution NMR can, in principle, determine dynamic amplitudes, and rates to atomic resolution, but in the case of DNA, results deduced from various types of NOE, scalar coupling, and relaxation studies are far from unanimous in their views. Each of the solution NMR methods mentioned has strengths and weaknesses when applied to studies of localized motions. NOE's between protons within furanose rings are sensitive to the averaged inverse 6th power of nuclear distances, $\langle 1/r^6 \rangle$, but

* To whom correspondence should be addressed.

(1) Saenger, W. *Principles of Nucleic Acid Structure*; Springer-Verlag New York, Inc.: New York, 1984.

(2) Dickerson, R. E.; Kopka, M. L.; Drew, H. R. *Structural Correlations in B-DNA*; Srinivasan, R., Sarma, R. H., Eds.; Adenine Press: New York, 1982; pp 227−257.

(3) Schomaker, V.; Trueblood, K. N. *Acta Crystallogr. Sect. B* **1968**, *24*, 63−76.

(4) Holbrook, S. R.; Kim, S.-H. *J. Mol. Biol.* **1984**, *173*, 361−388.

10.1021/ja010721d CCC: $20.00
Published on Web 09/25/2001

the exact nature of the averaging, or even its presence, can be obscured by spin diffusion effects. Scalar couplings can be related to dihedral angles within the context of a Karplus-like model, whose semiempirical extension to coupled protons in DNA is complicated by cross-relaxation.[5] Also, the small magnitudes of scalar couplings preclude an insight into the dynamic nature of furanose ring conformation. The so-called model-free relaxation analysis[6,7] is very widely used in protein studies, and several such studies of DNA dynamics have appeared.[8−10] Like all methods based on order parameters, model-free studies assume the local, internal motions in question occur on time scales widely separated from the overall molecular motion. For DNA duplexes on the order of 12 base pairs in length, this suggests that local motions of the furanose ring must occur on a time scale much less than a nanosecond. If this fails to be the case, order parameter studies will be less useful for accurately quantifying furanose ring dynamics.

Solid-state deuterium NMR brings its own particular strengths, weaknesses, and limitations to DNA studies. Its limitations are of a practical nature. It relies on selective isotopic labeling and thus cannot easily survey the wealth of sites accessible by crystallography and solution NMR. A strength of the technique is the wide dynamic range of motion that can be probed by solid-state NMR methods, a fact that follows directly from the broad solid-state NMR line width of deuterium (∼200 kHz).

The most common and simple models of furanose ring dynamics portray it as an exchange between two conformers,[11−14] although recent experimental analyses of proton scalar coupling constants in DNA assume exchange between a greater distribution of conformers.[15] Although activated exchange between discrete conformations of the furanose ring is a good approximation of internal molecular motions when kinetic barriers exceed 5.8 kcal/mol ($10k_BT$), theoretical estimates of the barrier to exchange between C2′-endo and C3′-endo (see Figure 1, parts a and b respectively) range from only 0.5 kcal/mol,[12] a remarkably low barrier indicating virtually free pseudorotation, to about 2−5 kcal/mol.[16] Therefore discrete site exchange may be a poor approximation for furanose ring motions in DNA. A more physically realistic model of furanose ring motion is almost certainly necessary for accurate analysis of NMR relaxation and line shape data.

In this paper we present a model of furanose ring dynamics in which angular displacements of C−D bonds are treated according to the Smoluchowski theory of Brownian motion through a potential barrier. Within the context of this theory, analysis of solid-state deuterium NMR equilibrium and nonequilibrium line shapes requires assumptions regarding the trajectories of the C−D bonds and the form of the potential barriers encountered as the C−D bonds move along these trajectories. We will show that solid-state deuterium line shapes vary markedly as a function of the assumed trajectories and potential barrier. Theoretically derived models of internal motion of DNA can thus be directly tested by solid-state deuterium NMR.

The sequence of interest for this particular study is [d(CGCGAATTCGCG)]$_2$, where C3 (underlined) is [2″-^{2}H]-2′-deoxycytidine, shown in Figure 1d. This sequence was the first successfully crystallized full turn of DNA in the B-form, performed by the Dickerson research group.[17] This sequence contains the binding site for the *EcoRI* restriction-modification system, −G↓AATTC−, where the "↓" indicates the cutting site for the endonuclease, and the underlined residue is the target for the methyltransferase. The structure and dynamics of this particular sequence have been studied extensively by numerous experimental techniques including X-ray crystallography,[4,17−19] atomic force microscopy,[20] solution NMR,[13,21−23] and solid-state NMR.[14,24−30] In particular, the furanose ring dynamics have been studied for this sequence in detail.[14,27−30]

We have obtained excellent fits for both equilibrium (fully relaxed) line shapes and nonequilibrium (partially relaxed) line shapes that demonstrate the utility of deuterium NMR for defining the trajectories and energetics of internal biomacromolecular motions in an exact and quantitative manner.

Materials and Methods

Chemical Synthesis of Selectively Deuterated DNA. To investigate furanose ring dynamics, [2″-^{2}H]-2′-deoxycytidine (Figure 1d) was prepared by the method of Robins et al. with some minor modifications to the solvent systems.[31] [2″-^{2}H]-2′-Deoxycytidine was converted to its N^4-benzoyl-5′-O-(DMT)-2′-dC-3′-CED-phosphoramidite derivative as described previously.[32] Oligonucleotides were synthesized by using an ABI Model 394 automated DNA/RNA synthesizer and purified on Sephadex size-exclusion columns as described previously, salted (10% NaCl by weight), packed into a 5 mm solid-state NMR Kel-F sample chamber, and hydrated by vapor diffusion in a humidity chamber containing saturated salts in ^{2}H-depleted water (75% relative humidity

(5) Zhu, L.; Reid, B. R.; Kennedy, M.; Drobny, G. P. *J. Magn. Reson., Ser. A* **1994**, *111*, 195−202.
(6) Lipari, G.; Szabo, A. *J. Am. Chem. Soc.* **1982**, *104*.
(7) Lipari, G.; Szabo, A. *J. Am. Chem. Soc.* **1982**, *104*.
(8) Eimer, W.; Williamson, J. R.; Boxer, S. G.; Pecora, R. *Biochemistry* **1990**, *29*, 799−811.
(9) Spielmann, H. P. *Biochemistry* **1988**, *27*, 5426−5438.
(10) Kojima, C.; Ono, A.; Kainosho, M.; James, T. L. *J. Magn. Reson.* **1998**, *135*, 310−333.
(11) Altona, C.; Sundaralingam, M. *J. Am. Chem. Soc.* **1972**, *94*, 8205−8212.
(12) Levitt, M.; Warshel, A. J. *J. Am. Chem. Soc.* **1978**, *100*, 2607−2613.
(13) Bax, A.; Lerner, L. *J. Magn. Reson.* **1988**, *79*, 429−438.
(14) Hatcher, M. E.; Mattielo, D. L.; Meints, G. A.; Orban, J.; Drobny, G. P. *J. Am. Chem. Soc.* **1998**, *120*, 9850−9862.
(15) Ulyanov, N. B.; Schmitz, U.; Kumar, A.; James, T. L. *Biophys. J.* **1995**, *68*, 13−24.
(16) Olson, W. K.; Sussman, J. L. *J. Am. Chem. Soc.* **1982**, *104*, 270−278.
(17) Dickerson, R. E.; Drew, H. R. *J. Mol. Biol.* **1981**, *149*, 761−786.
(18) Shui, X.; McFail-Isom, L.; Hu, G. G.; Williams, L. D. *Biochemistry* **1998**, *37*, 8341−8355.
(19) Shui, X.; Sines, C.; McFail-Isom, L.; Hu, G. G.; Williams, L. D. *Biochemistry* **1998**, *37*, 16877−16887.
(20) Garcia, R. A.; Bustamante, C. J.; Reich, N. O. *Proc. Natl. Acad. Sci., U.S.A.* **1996**, *93*, 7618−7622.
(21) Hare, D. H.; Wemmer, D. E.; Chou, S.-H.; Drobny, G. P.; Reid, B. R. *J. Mol. Biol.* **1983**, *171*, 319−336.
(22) Ott, J.; Eckstein, F. *Biochemistry* **1985**, *24*, 2530−2535.
(23) Nerdal, W.; Hare, D. R.; Reid, B. R. *Biochemistry* **1989**, *28*, 10008−10021.
(24) Mehta, M. A.; Gregory, D. M.; Kiihne, S.; Mitchell, D. J.; Hatcher, M. E.; Shiels, J. C.; Drobny, G. P. *Solid State Nuclear Magn. Reson.* **1996**, *7*, 211−228.
(25) Merritt, M. E.; Sigurdsson, S. T.; Drobny, G. P. *J. Am. Chem. Soc.* **1999**, *121*, 6070−6071.
(26) Gregory, D. M.; Mehta, M. A.; Shiels, J. C.; Drobny, G. P. *J. Chem. Phys.* **1997**, *107*, 28−42.
(27) Geahigan, K. B.; Meints, G. A.; Hatcher, M. E.; Orban, J.; Drobny, G. P. *Biochemistry* **2000**, *39*, 4939−4946.
(28) Hatcher, M. E. *A Solid-State Deuterium NMR Investigation of the Local Dynamics of Nucleotides in the EcoRI Restriction Endonuclease Binding Site*; University of Washington: Seattle, WA, 1996; p 138.
(29) Huang, W.-C.; Orban, J.; Kintanar, A.; Reid, B. R.; Drobny, G. P. *J. Am. Chem. Soc.* **1990**, *112*, 9059−9068.
(30) Meints, G. A. J. *An Investigation of Local DNA Dynamics in Bacterial Restriction Sites by Solid-State Deuterium NMR*; University of Washington: Seattle, WA, 2000; p 250.
(31) Robins, M. J.; Wilson, J. S.; Hansske, F. *J. Am. Chem. Soc.* **1983**, *105*, 4059−4065.
(32) Gait, M. J. *Oligonucleotide Synthesis: A Practical Approach*; Rickwood, D., Hames, B. D., Eds.; IRL Press: Oxford, Washington, D.C., 1984; p 217.

at 20 °C).[33] Water content was quantified gravimetrically by the parameter *W* (moles of water molecules/moles of nucleotide) and is accurate to ±1 water per nucleotide.

Solid-State NMR Spectroscopy. All experiments were performed on a home-built NMR spectrometer, operating at a deuterium Larmor frequency of 76.776 MHz, corresponding to a magnetic field strength of 11.75 T. A quadrupolar echo pulse sequence with an eight-step phase cycling scheme was implemented with a delay of 40 μs between 90° pulses (typically, 2.4−3.0 μs in duration) and a dwell time of 200 ns during acquisition. Data acquisition was initiated prior to the echo maximum. The time domain data were left-shifted and apodized with 3000 Hz Lorentzian line broadening prior to Fourier transformation. Partially relaxed line shapes and spin−lattice relaxation times were determined by using an inversion recovery pulse sequence, which incorporated a 180° composite pulse to ensure broadband excitation.[34] To obtain powder-averaged Zeeman spin−lattice relaxation times, $\langle T_{1Z} \rangle$, the integrated intensity of the powder spectrum was monitored as a function of recovery time and analyzed using a nonlinear least-squares fitting routine.[35] Please note that in all experimental spectra, the center isotropic peak is due to residual HDO.

Calculation of Dynamically Averaged Deuterium Line Shape Spectra. The geometry of the furanose ring is described by the positions of the 4 carbon atoms and the single oxygen atom, where the cyclic nature of the furanose ring actually reduces the number of independent geometrical parameters. The concept of pseudorotation was originated by Kilpatrick et al.[36] to treat the conformation of cyclopentane, and through the years has been adapted to a number of applications including the description by Altona et al. of the conformation of furanose rings in DNA.[11]

A number of general models of pseudorotational motion have been developed for furanose rings. In particular, Herzyk and Rabczenko[37] developed a general geometrical model of furanose ring conformation. This model predicts structures of the β-D-furanoside fragments that are in excellent agreement with crystal structures. The Cartesian coordinates of the *j*th atom in the furanose ring are, according to Herzyk and Rabczenko:

$$x_j = r_j\left[\sin 2\left(\varphi + \frac{4\pi j}{5}\right)\sin\alpha_j - \cos 2\left(\varphi + \frac{4\pi j}{5}\right)\cos\alpha_j\right] + R_j\cos\alpha_j \quad (1a)$$

$$y_j = -r_j\left[\sin 2\left(\varphi + \frac{4\pi j}{5}\right)\cos\alpha_j - \cos 2\left(\varphi + \frac{4\pi j}{5}\right)\sin\alpha_j\right] + R_j\sin\alpha_j \quad (1b)$$

$$z_j = \left(\frac{2}{5}\right)^{1/2} q\cos\left(\varphi + \frac{4\pi j}{5}\right) \quad (1c)$$

where α_j is the polar angle locating the *j*th bond, r_j is the radius of the projection of the pseudorotation trajectory onto the plane of the undistorted ring, R_j is the distance from the geometric center of the planar five-membered ring to the center of the projection of the *j*th trajectory onto the plane of the undistorted furanose ring, assumed to be circular in ideal pseudorotation (see Figure 2), *q* is the puckering amplitude (in Å), and φ is the pseudorotation phase. Because r_j and R_j can be determined from the geometry of the furanose ring (see eqs 3 and 4 from Herzyk and Rabczenko), eqs 1a−c reduce the dynamics of the furanose ring to two parameters, *q* and φ. If *q* is fixed, the motion of the furanose ring is only dependent upon φ.

Equation 1 describes the coordinates of the heavy atom framework of the furanose ring. However, the experimental data in this deuterium NMR study are not obtained for a member of the furanose ring itself, but rather for a deuterium substituent at the 2″ site (see Figure 1d).

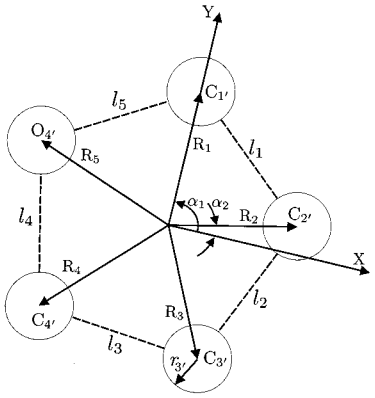

Figure 2. Representation of the projection of the furanose ring atomic trajectories during rigid pseudorotation. Adapted from ref 37.

We have used an extension of the basic model of Herzyk and Rabczenko to generate atomic coordinates for each ring substituent, and specifically for the deuterium atom at the 2″ site. This extension of the Herzyk−Rabczenko model simply assumes that the carbons in the ring are sp^3 hybridized, i.e., the bond configuration has tetrahedral symmetry.

To calculate and visualize the furanose ring trajectories, we used a C++ software library, molecular tool kit (mtk).[38] The mtk library allows the modeling of molecules similar to a plastic "ball-and-stick" model. In such a model, each atom has a certain configuration of "holes", reflecting the allowed bond hybridization. In the case of carbon, this configuration is typically tetrahedral. Tetrahedral symmetry implies that if the geometry of two bonds to a single carbon is known, then the configuration of the other two bonds can be calculated, based upon the known ones. The carbon element in the mtk library supports by default tetrahedral symmetry and the coordinates for a substituent attached to such a carbon may therefore easily be extracted. In this particular case, the carbon tetrahedral symmetry is oriented to first satisfy the geometry of the ring itself, as calculated from the pseudorotation coordinates *q* and φ, then the coordinates of any substituent are calculated.

With these assumptions we have determined furanose ring dynamics in terms of the trajectory of the deuterium atoms (Figure 3a). In Figure 3b, multiple trajectories of the 2″ deuteron are displayed as a function of the puckering amplitude *q*. In Figure 3c,d, corresponding trajectories are shown for the 2′ carbon atom.

To simulate the solid-state deuterium NMR line shape we need to transform the Electric Field Gradient (EFG) tensor from the frame of its Principal Axis System (PAS) to a molecular fixed frame (MF).[39] The deuterium high-field quadrupolar coupling Hamiltonian is given by

$$H_Q = \frac{eQ}{2h}\tilde{I}\cdot\tilde{V}\cdot\tilde{I} \quad (2)$$

where *Q* is the nuclear quadrupole moment, $\tilde{I}$ is the nuclear spin angular momentum operator, and $\tilde{V}$ is the electric field gradient (EFG) tensor. For a deuterium nucleus the *z*-axis of the principal axis system (PAS) of the EFG tensor is parallel to the C−D bond axis. The deuterium EFG tensor is approximately axial and has the form

$$V_{\mathrm{PAS}} = \frac{eq}{2}\begin{pmatrix} 1 & 0 & 0 \\ 0 & 1 & 0 \\ 0 & 0 & -2 \end{pmatrix} \quad (3)$$

where *q* is the field gradient. The molecular-fixed (MF) frame, defined in Figure 2, is related to the coordinates of the heavy atoms of a planar (and fictitious) furanose ring.

(33) Weast, R. C. *CRC Handbook of Chemistry and Physics*, 60th ed.; Boca Raton, FL, 1979.
(34) Tycko, R. *Phys. Rev. Lett.* **1983**, *51*, 775−777.
(35) deFontaine, D. L.; Ross, D. L.; Ternai, B. J. *J. Magn. Reson.* **1975**, *18*, 276.
(36) Kilpatrick, J. E.; Pitzer, K. S.; Spitzer, R. *J. Am. Chem. Soc.* **1947**, *69*, 2483−2488.
(37) Herzyk, P.; Rabczenko, A. *J. Chem. Soc., Perkin Trans. 2* **1985**, 1925−1930.
(38) Karlsson, T.; Levitt, M. H. *Moleculix, an interactive visualization and simulation software package*; Poster presentation at Experimental NMR Conference, 2000.
(39) Abragam, A. *Principles of Nuclear Magnetism*; Oxford University Press: New York, 1961.

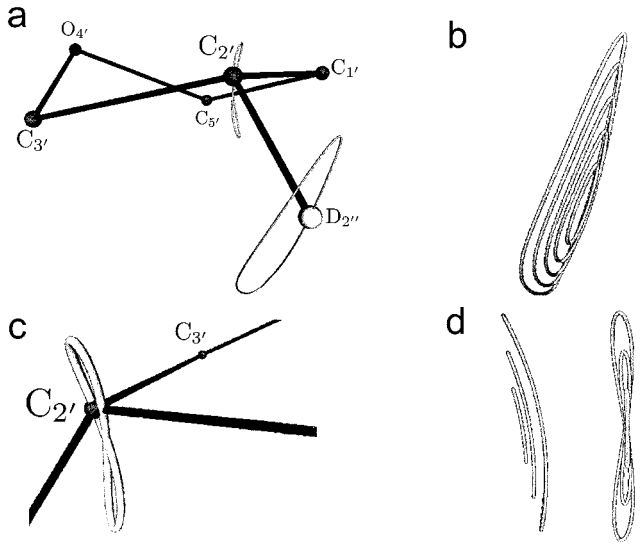

Figure 3. Calculated carbon and deuterium trajectories. (a). Trajectory of the 2″ deuteron for the puckering amplitude $q = 0.4$ Å, along with the associated 2′ carbon trajectory. (b) Deuterium trajectories as a function of puckering amplitude q. (c) Enlarged view of the carbon trajectory at puckering amplitude $q = 0.4$ Å. Note the figure eight shape. (d) Enlarged view of the carbon trajectories as a function of puckering amplitude q. Note that two different views are shown.

Since the EFG tensor is assumed to be axially symmetric, only two Euler angles, θ and ϕ, are needed to describe the transformation from the PAS frame to the MF frame. The angles θ and ϕ were calculated by the mtk library as a function of puckering amplitudes q and puckering phase φ, and subsequently fed into the deuterium line shape simulation program.

Analysis of equilibrium and nonequilibrium solid-state deuterium NMR line shapes follows the equation of motion for the transverse magnetization of the spin 1 nucleus:

$$\frac{dM_{\pm}}{dt} = [i\omega_{\pm}(\Omega) + R(\Omega)]M_{\pm} \tag{4}$$

where the "+" refers to the $0 \rightarrow +1$ transition and the "−" refers to the $-1 \rightarrow 0$ transition. $R(\Omega)$ is an operator that describes the specific dynamics in question, and may be represented as a linear operator in the case of continuous motions or as a matrix in the case of discrete jumps. Ω is the solid angle that relates the principal axis (PAS) frame of the EFG tensor to the lab-fixed frame. Because the EFG tensor is approximately symmetric, a single static angle θ relates its PAS frame to the static field direction. Hence the angular dependent frequencies are:

$$\omega_{\pm} = \pm\frac{3}{4}\frac{e^2qQ}{h}P_2(\cos\theta) \tag{5}$$

where e^2qQ is the quadrupolar coupling constant, h is Planck's constant, and $P_2(\cos\theta)$ is the second-order Legendre polynomial. Molecular motion modulates θ and thus additional transformations are required to one or more frames intermediate to the PAS frame and the LAB frame. The form of these additional transformations is obtained by using the addition properties of spherical harmonics.[40]

It remains to assume a form of the operator $R(\Omega)$. If the pseudorotation motions were freely diffusive, $R(\Omega)$ would simply be the three-dimensional diffusion operator

$$D\nabla^2 = D\left(\frac{\partial^2}{\partial x^2} + \frac{\partial^2}{\partial y^2} + \frac{\partial^2}{\partial z^2}\right) \tag{6}$$

where D is the diffusion coefficient associated with the stochastic motion of the C−D bind. As mentioned, a large body of theoretical and empirical data argue that there are significant energy barriers to structural changes in furanose rings.

A form of Smoluchowski's diffusion equation

$$\frac{\partial P}{\partial t} = D\left[\frac{\partial^2}{\partial\varphi^2} + \frac{1}{k_BT}U'(\varphi)\frac{\partial}{\partial\varphi} + \frac{1}{k_BT}U''(\varphi)\right]P \tag{7}$$

has been used to describe the motion of heme groups in proteins,[41] amino acid side chains in proteins,[42] and lipid chains.[43] In eq 7, φ is the pseudorotation phase angle, $U(\varphi)$ is the potential energy as a function of φ, and P is the orientation probability distribution for a C−D bond. Note that by using the pseudorotation phase, the problem has been rendered in 1-dimensional form. For the purpose of solving eq 4 numerically, the operator

$$R(\varphi) = D\left[\frac{\partial^2}{\partial\varphi^2} + \frac{1}{k_BT}U'(\varphi)\frac{\partial}{\partial\varphi} + \frac{1}{k_BT}U''(\varphi)\right] \tag{8}$$

can be discretized. Following the procedure of Nadler and Schulten,[44] R can be represented by a matrix with elements

$$R_{ij} = \frac{1}{\tau_c}\sqrt{\frac{P_i}{P_{i\pm1}}}, \quad j = i \pm 1$$

$$R_{ij} = -(R_{i,i-1} + R_{i,i+1}), \quad j = i \tag{9}$$

$$R_{ij} = 0, \text{ otherwise}$$

where P_i is the a priori probability given as

$$P_i = \frac{e^{-U(\varphi_i)/k_BT}}{Z} \tag{10}$$

where

$$Z = \sum_i e^{-U(\varphi_i)/k_BT} \tag{10a}$$

and τ_c is the correlation time. We may express the correlation time τ_c in terms of the diffusion coefficient, D, or the kinetic rate constant k and a unit angular step δ as

$$\frac{1}{2\tau_c} = D = \frac{k\delta^2}{2} \tag{11}$$

It should be noted that the diffusion coefficient D is not for motion between two sugar conformations, but for an excursion along the energetic pathway, i.e., between two adjacent and discrete sites along the trajectory. Discussion of rates between sugar conformations is given in the Conclusion.

To simulate the deuterium line shape of the mobile C2′−D bond, a form of the potential $U(\varphi)$ must be chosen. Theoretical studies of the conformational dynamics of furanose rings in DNA and RNA assume a double-well potential,[1,12] with well minima closely corresponding to the C2′-endo and C3′-endo configurations of the furanose ring, shown in Figure 1.

A simple approximation to a double well potential has the form

$$U(\varphi) = \frac{U_0}{2}(1 - \cos 2\varphi) \tag{12}$$

where U_0 is the barrier height. Assuming values for U_0, a puckering amplitude q, angles θ and ϕ for each of the 10 sites (determined by

(40) Brink, D. M.; Satchler, G. R. *Angular Momentum*; Oxford University Press: London, 1968.

(41) Nadler, W.; Schulten, K. *Proc. Natl. Acad. Sci.* **1984**, *81*, 5719−5723.

(42) Wittebort, R. J.; Szabo, A. *J. Chem. Phys.* **1978**, *69*, 1722−1736.

(43) Wittebort, R. J.; Olejniczak, E. T.; Griffin, R. G. *J. Chem. Phys.* **1987**, *86*, 5411−5420.

(44) Nadler, W.; Schulten, K. *J. Chem. Phys.* **1986**, *84*, 4015−4025.

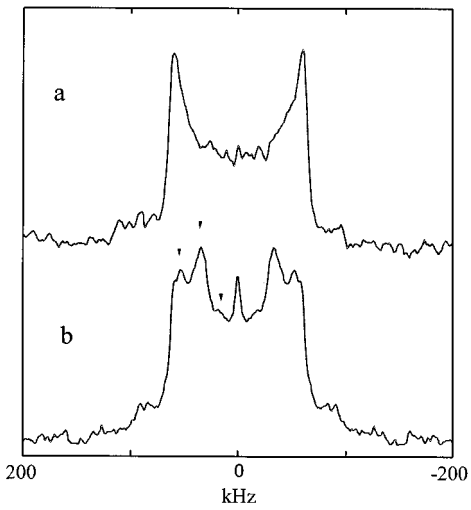

Figure 4. Line shapes for (a) [2″-^{2}H]-C3 (underlined) from [d(CGC-GAATTCGCG)]$_2$ with $W = 6$ and (b) [2″-^{2}H]-C3 with $W = 11.6$ (symmetrized). Note the three distinct spectral peaks indicated by the arrows; the center isotropic peak is due to residual HDO.

the trajectory calculations mentioned above), and the diffusion coefficient D, a motionally averaged deuterium line shape can be calculated. More complicated forms for $U(\varphi)$ may be obtained by expanding in a Fourier series in φ and truncating at appropriate orders, or raising the baseline of the potential surface. Truncated forms for $U(\varphi)$ will be investigated in addition to the potential in eq 12.

A natural approach would be to assume that pseudorotation involves exchanges between a discrete number of sites on the pseudorotation trajectory. In some cases, only two sites are assumed,[14] but this has produced poor results for simulating solid-state deuterium NMR spectra. For our simulations we have discretized a trajectory for the furanose ring to 10 sites, which is a sufficient number to effectively simulate a continuous process as has been shown,[43,45] and site populations are determined by eq 10. For an N-site exchange process, eq 4 becomes

$$\dot{M}_{j,\pm} = \sum_{k=1}^{N} (i\omega_{j\pm}\delta_{jk} + R_{jk})M_{k,\pm} \tag{13}$$

where the complex transverse magnetization $M_\pm = M_{X,\pm} + iM_{Y,\pm}$. The coherence frequency ω_i is a function of the angles θ and ϕ and the angles (Φ,Θ) that relate the molecule-fixed frame to the lab frame, i.e.

$$\omega_{\pm,i} = \mp\frac{3}{4}\frac{e^2qQ}{\hbar}\left[\frac{1}{4}(3\cos^2\theta - 1)\cdot(3\cos^2\theta - 1) - \frac{3}{4}\sin 2\Theta\cdot\cos(\phi_i + \Phi) + \frac{3}{4}\sin^2\theta\cdot\sin^2\Theta\cdot\cos 2(\phi_i + \Theta)\right] \tag{14}$$

and the matrix elements R_{ij} are given by eq 9. Numerical solutions to eq 13 were accomplished with the program MXET1, developed by the Vold group.[46,47] Please note that center spikes in all simulated spectra are due to dc offset.

Results and Discussion

Deuterium Line Shape and Relaxation Data for the 2″ Deuteron in C3. Figure 4a,b shows the C3 line shape at hydration levels $W = 6$ and 11.6, respectively. The classic Pake doublet is visible in the lower hydration level only (Figure 4a), and is lost upon increased hydration (Figure 4 b), where there is significant motional averaging. The horns of the spectrum have shrunk, and there are three distinct spectral peaks visible within (indicated by arrows). The sharp middle peak is from residual HDO. The spin−lattice relaxation time, $\langle T_{1Z}\rangle$, was determined to be 42 ± 5 ms, and a series of partially relaxed line shapes are shown in Figure 11a.

Types of DNA Motion. In addition to simulating the motion of the particular sugar ring in question, it is necessary to resolve other types of motion that are present in the sample. Hydrated solids have numerous advantages when resolving DNA motions. Bending and torsional motions can be neglected for short DNAs.[45] Also, end-to-end tumbling can be neglected, as this type of motion is restricted in the solid state, even with a sample of intermediate hydration ($10 < W < 20$). Last, there is simple rotation around the helical axis. Previous work has shown that this rotation is effectively simulated by a six-site jump,[45] with a half angle of $\theta = 20°$ (orientation of the C2′−D bond with respect to the longitudinal helix axis), values of $\phi = 0°$, 60°, 120°, 180°, 240°, and 300° for the six sites, and a rate constant of $k = 10^4$ Hz. Use of these parameters for the overall helix motion has produced good agreement in previous work for several different DNA samples with different types of local motions occurring.[14,45] Therefore, these parameters will be considered well determined and remain constant for our simulations of the local motions. The resulting spectra will then be a superposition of this longitudinal helical rotation and the local motion of the furanose ring.

Simulations of Furanose Ring Dynamics with Use of the Brownian Trajectory Model. The first step toward developing a dynamical model for comparison to experimental data is to determine the model's dependence on the various adjustable parameters. There are several adjustable parameters within the simulations, including the diffusion coefficient D, the puckering amplitude q (which determines the spatial position and the trajectories of the atoms in the sugar ring), and the actual form of the potential $U(\varphi)$. We have generated a library of simulations to illustrate the dependence of our model upon these adjustable parameters.

Figure 5a−c illustrates the forms of the first three potentials we have used for our simulations. Figure 5a shows a double well potential with equal barrier heights, described analytically by eq 12. Figure 5b shows a double well potential with unequal barrier heights, as described in eq 15. Figure 5c shows a potential described by eq 16, which is a second-order truncation of the Fourier series. Particular simulations will refer to these to indicate the form of the utilized potential energy surface.

Figure 6a−e shows a series of deuterium line shape simulations, varying the φ-independent diffusion coefficient, D, between adjacent and discrete coordinates along the trajectory. Figure 6 shows the model's dependence on D by varying the coefficient over several simulations, from a value of $D = 1.9 \times 10^5$ kHz (Figure 6a) to 1.9×10^9 kHz (Figure 6e). The puckering amplitude is fixed at $q = 0.4$ Å, the potential is described by eq 12 and Figure 6a, and the barrier height is fixed at $U_0 = 5k_BT$ (~2.9 kcal/mol). There is a dependence of the line shapes upon this parameter observed over several orders of magnitude.

Figure 6f−j shows a series of simulations as a function of the puckering amplitude q, from a value of $q = 0.2$ Å (Figure 6j) to $q = 0.6$ Å (Figure 6j), while keeping the parameters $D = 9.9 \times 10^8$ Hz and $U_0 = 5k_BT$ constant, and the potential is described by eq 12 and Figure 5a. There is a dramatic dependence on this parameter, which is fundamentally a measure of amplitude of the furanose motion. The motion of the deuteron

(45) Alam, T. M.; Drobny, G. P. *Chem. Rev.* **1991**, *91*, 1545−1590.
(46) Greenfield, M. S.; Ronemus, A. D.; Vold, R. L.; Vold, R. R.; Ellis, P. D.; Raidy, T. E. *J. Magn. Reson.* **1987**, *72*, 89−107.
(47) Vold, R. R.; Vold, R., L. *Deuterium Relaxation in Molecular Solids*; Academic Press: San Diego, 1991; Vol. 16, pp 85−171.

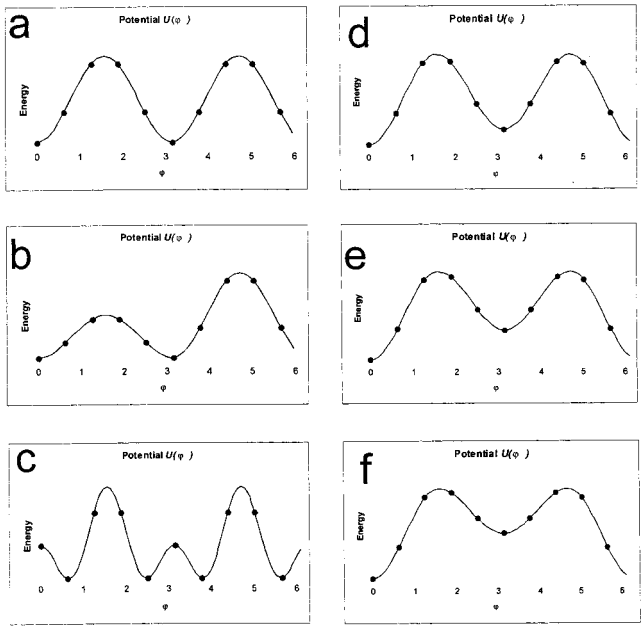

Figure 5. Graphs of the analytical forms of the different potentials used in this investigation: (a) for eq 12 representing an equal double well potential, (b) for eq 15 representing a double well potential with unequal barrier heights, and (c) for eq 16 representing the second-order truncation of the Fourier series. A series of potential energy surfaces, d−f, where the one of the two wells is raised relative to the other, but the barrier heights are kept equal. The baseline has been raised from zero to approximately (d) 1/6 the height of the barrier, (e) 1/3 the height of the barrier, and (f) 1/2 the height of the barrier. The barrier heights have remained equal at a value of $U_0 = 5k_BT$ (2.9 kcal/mol), so the baseline has been raised to approximately (d) 0.5, (e) 1, and (f) 1.5 kcal/mol, respectively.

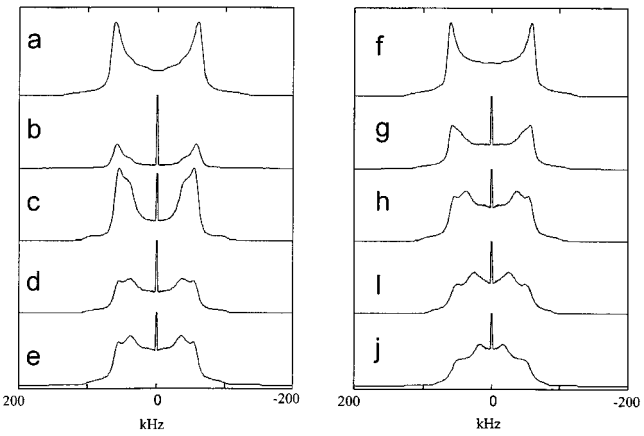

Figure 6. A series of simulations, a−e (discussed in the text), varying the diffusion coefficient, D, for the potential $U(\varphi) = (U_0/2)(1 - \cos 2\varphi)$ with $U_0 = 5k_BT$: (a) $D = 1.9 \times 10^5$ Hz, (b) $D = 1.9 \times 10^6$ Hz, (c) $D = 1.9 \times 10^7$ Hz, (d) $D = 1.9 \times 10^8$ Hz, and (e) $D = 1.9 \times 10^9$ Hz. The constant parameters are a puckering amplitude $q = 0.4$ Å and $U_0 = 5k_BT$. A series of simulations f−j (discussed in the text) varying the puckering amplitude q, for the potential $U(\varphi) = (U_0/2)(1 - \cos 2\varphi)$: (f) $q = 0.2$ Å, (g) $q = 0.3$ Å, (h) $q = 0.4$ Å, (i) $q = 0.5$ Å, and (j) $q = 0.6$ Å. The constant parameters are diffusion coefficient $D = 9.9 \times 10^8$ Hz and $U_0 = 5k_BT$.

increases as the puckering amplitude increases, and this is exhibited as increased motional averaging of the deuterium line shape.

Figure 7a−d shows four series of partially relaxed simulated spectra corresponding to barrier heights U_0 of $4k_BT$, $5k_BT$, $5.5k_BT$, and $6k_BT$, respectively. The null of the relaxation inversion has a distinct dependence on the potential barrier height. This indicates that analysis of the barrier height will be a significant tool for determining an accurate model and parameter set to simulate experimental data. Table 1 summarizes the $\langle T_{1Z} \rangle$ values calculated by integration of the partially relaxed simulated spectra and fitting to an exponential curve.

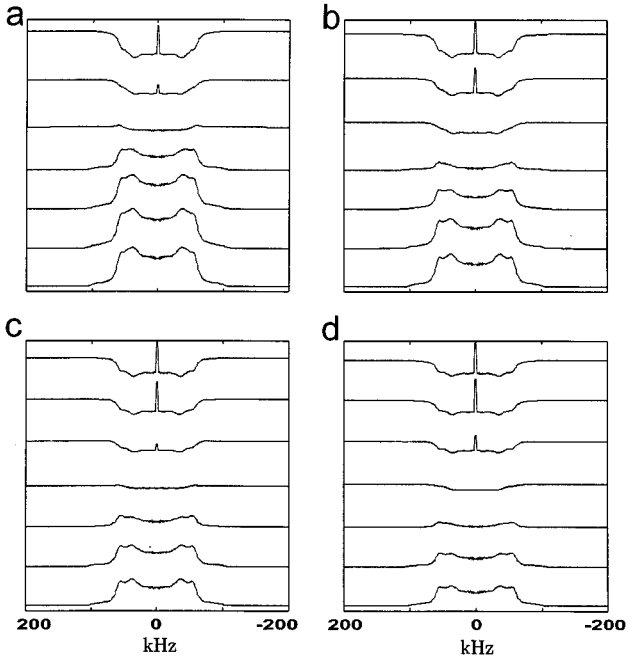

Figure 7. A series of partially relaxed simulated line shapes varying the height of equal potential barriers. The barrier heights are (a) $U_0 = 4k_BT$, (b) $U_0 = 5k_BT$, (c) $U_0 = 5.5k_BT$, and (d) $U_0 = 6k_BT$. Note that the null of the inversion (crossover point) has a distinct dependence on the barrier height. The constant parameters are diffusion coefficient $D = 9.9 \times 10^8$ Hz and puckering amplitude $q = 0.4$ Å.

Table 1. Comparison of Spin−Lattice Relaxation Times[a]

DNA sample or potential barrier height for simulations	$\langle T_{1Z} \rangle$, ms
[2″-^{2}H]-C3 (underlined) from the DNA sequence, [d(CGCGAATTCGCG)]$_2$	42 ± 5
$2 \times 4k_BT$	19
$2 \times 5k_BT$	34
$2 \times 5.5k_BT$	47
$2 \times 6k_BT$	65

[a] A series of spin−lattice relaxation times, for [2″-^{2}H]-C3 (underlined) from the DNA sequence [d(CGCGAATTCGCG)]$_2$, compared to several simulations with variable but equal potential barrier heights. The simulations vary the barrier height U_0 for the potential form $U(\varphi) = (U_0/2)(1 - \cos 2\varphi)$, from eq 12. The constant parameters are diffusion coefficient $D = 9.9 \times 10^8$ Hz and puckering amplitude $q = 0.4$ Å.

In many studies of furanose ring motion, the barriers for the double well potential are unequal. For example, Levit and Warshel calculated a barrier of <2 kcal/mol at O1′-endo, near a pseudorotation phase angle of 90−100°.[12] Olson and Sussman proposed a potential energy function that was used to estimate the pseudorotational motions of ribose and 2′-deoxyribose sugars.[16] This potential, which included nonbonded, torsional, and valence angle strain contributions in addition to an intrinsic gauche energy term to account for the puckering preferences, was (for 2′-deoxyribose) essentially a double well potential with barriers of 2 kcal/mol at a pseudorotation phase angle of about 70−75°, and a second barrier of about 6 kcal/mol at a pseudorotation phase angle of roughly 270°.

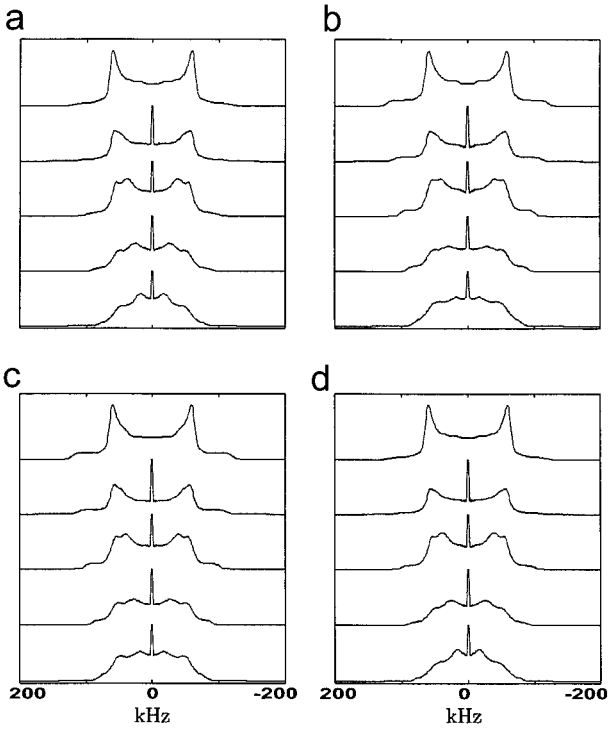

Figure 8. A series of simulations (discussed in the text) using eq 15 to describe the potential energy surface, where one of the two barriers is larger for a double well potential. For these simulations, one barrier remains at $5k_BT$, and other is varied from (a) $6k_BT$, (b) $7k_BT$, (c) $8k_BT$, and (d) $10k_BT$. The constant parameters are diffusion coefficient $D = 9.9 \times 10^8$ Hz and varying the puckering amplitude in each set from $q = 0.2$ to 0.6 Å, in steps of 0.1 Å, from top to bottom.

For simulations using an unequal double well potential, we have used the following analytical form,

$$U(\varphi) = \frac{U_{0_1}}{2}(1 - \cos 2\varphi), \quad 0 < \varphi < \pi \tag{15a}$$

$$U(\varphi) = \frac{U_{0_2}}{2}(1 - \cos 2\varphi), \quad \pi < \varphi < 2\pi \tag{15b}$$

Equation 13 is shown graphically in Figure 5b. Figure 8a−d shows a series of simulations where one of the two barriers has its amplitude (U_0) varied from $6k_BT$ (Figure 8a) to $10k_BT$ (Figure 8d), while the height of the second barrier parameter remains constant at $5k_BT$. The puckering amplitude ranges from $q = 0.2$ Å, for the top simulations, to $q = 0.6$ Å, for the bottom in increments of 0.1, and the diffusion coefficient remains constant at $D = 9.9 \times 10^8$ Hz. For the simulations with a $5k_BT$ and $6k_BT$ barrier, as well as $5k_BT$ and $10k_BT$, there is little deviation from the forms of the line shapes with equal $5k_BT$ barriers (Figure 6), but with a $7k_BT$ or $8k_BT$ height for the second barrier, there is a noticeable difference for larger values of the puckering amplitude q.

The potential function shown in eq 15 and Figure 5b is a simple approximation of the potential surface proposed by Levitt and Warshel[12] and Olson.[16] Such potentials have been proposed in part on the basis of X-ray crystallography data, which indicated the furanose structures are clustered tightly around the 2-endo and 3-endo configurations, and by NMR scalar coupling data, which similarly support the existence of two dominant equilibrium conformations. Ulyanov et al. presents a statistical analysis of scalar couplings in DNA furanose rings that support the existence of more than two equilibrium conformations of the furanose ring.[15] To investigate the possibility of such effects, a form for $U(\varphi)$ truncated to "second order" is explored:

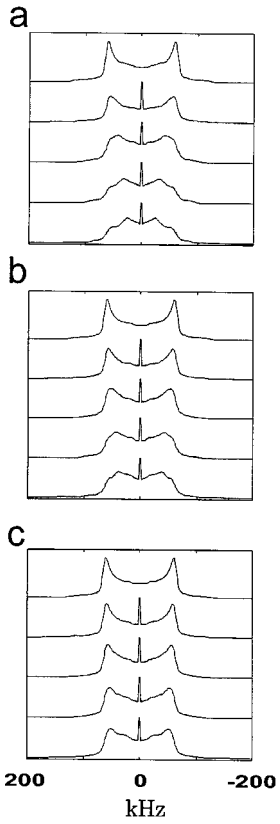

Figure 9. A series of simulations (discussed in the text) using the potential energy surfaces from Figure 5d−f. The well depth has been raised from zero to approximately (a) 0.5, (b) 1, and (c) 1.5 kcal/mol. The simulation parameters are $D = 9.9 \times 10^8$ Hz, $U_0 = 5k_BT$ (2.9 kcal/mol), and varying the puckering amplitude in each set from $q = 0.2$ to 0.6 Å, in steps of 0.1 Å from top to bottom.

$$U(\varphi) = \frac{U_0}{2}(1 - (\cos 2\varphi + \cos 4\varphi)) \tag{16}$$

A graph of the angular dependence of the potential in eq 16 is shown in Figure 5c.

Finally, simulations have shown dependence upon raising the baseline of one well with the potential relative to the other well. Figure 5d−f shows a series of potentials where the baseline has been raised from zero to approximately (d) $^1/_6$ the height of the barrier, (e) $^1/_3$ the height of the barrier, and (f) $^1/_2$ the height of the barrier. The barrier heights have remained equal at a value of $U_0 = 5k_BT$ (2.9 kcal/mol), so the baseline has been raised to approximately (d) 0.5, (e) 1, and (f) 1.5 kcal/mol, respectively. Parts a, b, and c in Figure 9 are series of simulations corresponding to the aforementioned potentials (i.e. from Figure 5, parts d, e, and f, respectively), with the diffusion coefficient $D = 9.9 \times 10^8$ Hz and the puckering amplitude $q = 0.4$ Å. As can be seen there is indeed a dependence upon having unequal potential well depths as well as unequal potential barrier heights.

Comparison of Experimental Spectra to Simulations. Previous work has shown fair agreement between a motionally averaged line shape for [2″-^{2}H]-C9 from the Dickerson sequence and a two-site jump model for the furanose ring motion, with a half-angle amplitude of 38°.[14] While there was reasonable agreement between the fully relaxed experimental line shape

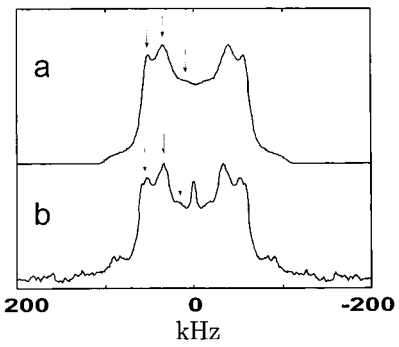

Figure 10. Best-fit comparison of simulation to experiment. (a) Simulation using the following parameters: potential $U(\varphi) = (U_0/2)(1 - \cos 2\varphi)$, barrier magnitude $U_0 = 5.5k_BT$, diffusion coefficient $D = 9.9 \times 10^8$, and puckering amplitude $q = 0.4$ Å. (b) [2″-^{2}H]-C3 (underlined) from [d(CGCGAATTCGCG)]$_2$ with $W = 11.6$ (symmetrized).

and the two-site jump simulation, the model could not effectively simulate nonequilibrium (partially relaxed) line shapes. Additionally, a Brownian diffusion model with a single axis of angular motion has shown success simulating equilibrium, motionally averaged line shapes, but also could not accurately simulate partially relaxed line shapes.[27,30] Now it becomes necessary to utilize our new model to attempt to obtain accurate simulations of experimental data.

Figure 10 shows a best-fit comparison for the fully relaxed (equilibrium) line shape for C3 at $W = 11.6$ (Figure 4b). The parameters for this simulation are a diffusion coefficient $D = 9.9 \times 10^8$ Hz, puckering amplitude $q = 0.4$ Å, and an equal, double-well potential with equal wells and equal barrier heights of $U_0 = 5.5k_BT$. As can be seen, there is excellent agreement, even down to the small details of the experimental data. The three peaks (arrows in Figure 11) observed in the experimental spectrum are replicated in the simulated spectrum. As found from simulations, the equilibrium line shape does not have a dramatic dependence on the barrier height. However, Figure 7a−d and Table 1 show that the relaxation pattern does have a great dependence on the barrier height.

Figure 11 shows a direct comparison of (a) the partially relaxed experimental line shapes for C3 at $W = 11.6$ and (b) the partially relaxed simulated line shapes with identical delay times. The simulation parameters are identical to those in Figure 11. Additionally, the $\langle T_{1Z}\rangle$ of C3 at $W = 11.6$ was found to be 42 ± 5 ms, which can be compared to relaxation times for simulations from Table 1, where our model with the best fit parameters has a $\langle T_{1Z}\rangle$ of 47 ms. When comparing the fully and partially relaxed experimental line shapes with the best fit simulations, as well as the $\langle T_{1Z}\rangle$ values, we conclude that the C3 furanose ring is diffusing through a double $5.5k_BT$ barrier (~2.9 kcal/mol), with a puckering amplitude of 0.4 Å and a diffusion coefficient of 9.9×10^8 Hz. A discussion of the physical relevance of these simulation parameters follows.

Conclusions

The ultimate goal is to use this model to determine the dynamics of any furanose ring, as determined from solid-state deuterium NMR. It is now necessary to look at the utility of the model for simulating different line shapes. When the amplitudes of motion are small (<20°), or in the slow motion regime ($<10^6$ Hz), it is not easy to distinguish one simulation from another (one can compare parts a and f of Figure 6 as examples). However, one can, upon inspection, determine that the furanose ring motions are in these regimes.

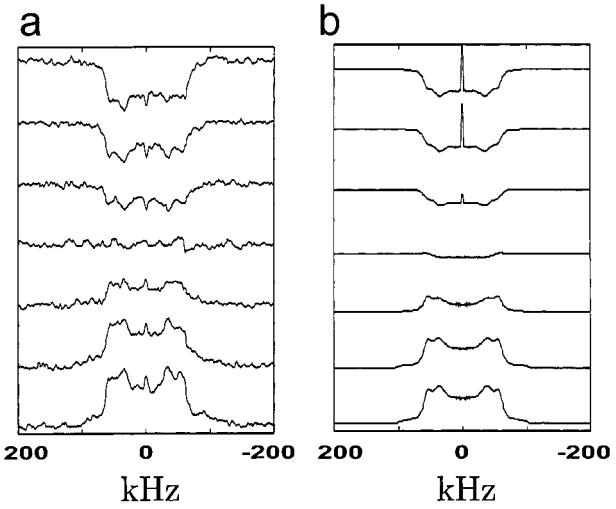

Figure 11. Comparison of the partially relaxed line shapes with identical relaxation delays which correspond to the experiment and simulation from Figure 16. Note that the variable delay times are as follows (from top to bottom): 1, 5, 10, 25, 50, 100, and 200 ms. The null of the inversion, where there is the greatest sensitivity to the model utilized, shows excellent agreement.

The utility of this model arises when the motions are in the large amplitude (>30°) and intermediate time scale regime (~10^6−10^8 Hz). This model shows a great dependence on its parameters in these regimes, as illustrated in the series of simulations in Figure 6. Line shape inspection and comparison can be used initially to determine general magnitudes of the amplitude of angular motion and the time scale of these motions. However, if one surveys the library of simulations presented, there is often a similarity between simulated line shapes with different parameters. Therefore, a second means to distinguish simulations from each other becomes necessary, namely to utilize the relaxation information from partially relaxed line shapes and spin−lattice relaxation times.

For example, if one wanted to compare the simulations shown in parts d and e of Figure 6 (which differ in their value for the diffusion coefficient D from 1.9×10^8 Hz to 1.9×10^9 Hz, respectively) to experimental data, differences between their equilibrium line shapes might be easily obscured under the spectral noise in the experimental data. However, their spin−lattice relaxation times, $\langle T_{1Z}\rangle$ values, are very different, with values of $\langle T_{1Z}\rangle = 89$ ms for the simulation in Figure 6d ($D = 1.9 \times 10^8$ Hz) and $\langle T_{1Z}\rangle = 18$ ms for the simulation in Figure 6e ($D = 1.9 \times 10^9$ Hz).

A comparison of relaxation information is useful for determining a reasonable potential energy surface as well. The question remains to be asked whether a certain form for the potential can be discerned from another, and if there is a better fit when comparing to actual spectroscopic data. One can use line shape inspection again to obtain a general idea of parameter values, as there is a dependence upon unequal barrier heights with a very large value for the puckering amplitude ($q > 0.4$ Å), as shown in Figure 8. However, when the puckering amplitude is smaller ($q \leq 0.4$ Å), the line shapes are not easily distinguished. Therefore an investigation of the relaxation parameters is necessary. Table 2 indicates the $\langle T_{1Z}\rangle$ values for several forms of the potential, $U(\varphi)$, and shows there is a distinct dependence of the relaxation on the barrier height of an unequal barrier. The model shows a marked dependence of the equilibrium line shapes upon relative changes in well depth as well, indicated in Figure 10.

Table 2. Comparison of Spin−Lattice Relaxation Times for Simulations with Different Relative Barrier Heights[a]

form of simulated potential energy surface	$\langle T_{1Z} \rangle$, ms
equal double barrier with $U_0 = 5k_BT$ (2.9 kcal/mol)	34
unequal double barrier with $U_{0,1} = 5k_BT$ and $U_{0,2} = 6k_BT$ (3.6 kcal/mol)	45
unequal double barrier with $U_{0,1} = 5k_BT$ and $U_{0,2} = 7k_BT$ (4.2 kcal/mol)	54
unequal double barrier with $U_{0,1} = 5k_BT$ and $U_{0,2} = 8k_BT$ (4.8 kcal/mol)	58
unequal double barrier with $U_{0,1} = 5k_BT$ and $U_{0,2} = 10k_BT$ (6 kcal/mol)	59

[a] A series of spin−lattice relaxation times for different potentials. The potentials are of double well form, where one barrier height remains constant at $5k_BT$, while the other varies relative to that value, varied from $6k_BT$ to $10k_BT$, as described by eq 15. The constant parameters are diffusion coefficient $D = 9.9 \times 10^8$ and puckering amplitude of $q = 0.4$ Å.

The results from our current work show good agreement between simulations using our model and our experimental data, as seen in Figures 10 and 11. There is still the possibility of simulation overlap, and while the work cannot conclusively state that our model is an exact replication of the dynamics present in the furanose ring, it can be used to eliminate models that do not accurately replicate the experimental data. However, the results from this model have shown the best agreement to date for replicating dynamically averaged deuterium line shapes from furanose labeled DNA's.

The utility of this model also allows for determination of rates between overall puckering conformations as well. The rate at which the C2′−D2″ bond passes over a barrier U_0 can also be estimated following the treatment of Edholm and Blomberg,[48] where the "escape" rate or the rate of passage over the barrier is approximated by,

$$\text{rate} \approx \left[-\left[\frac{\partial^2 U(\varphi)}{\partial \varphi^2} \right]_{\text{top}} \left[\frac{\partial^2 U(\varphi)}{\partial \varphi^2} \right]_{\text{bottom}} \right]^{1/2} \frac{D}{2\pi k_B T} \exp\left(-\frac{U_{\text{top}}}{k_B T} \right) \tag{17}$$

For our best fit, shown in Figure 10a,b, the simulations have a potential with equal barrier heights and equal well depths, where the barrier height is $U_0 = 5.5k_BT$, a puckering amplitude of $q = 0.4$ Å, and a diffusion coefficient of $D = 9.9 \times 10^8$. Using these parameters in calculating eq 15, we obtain an escape rate of 0.7×10^7 Hz, which is in the intermediate time regime, where it is expected to observe significant motional averaging for large amplitude motions. Additionally, it is similar to the rate between sites when a two-site jump model has been used previously to describe large amplitude motions in the furanose ring of C9 from the same DNA sequence,[14] whose value was 2.5×10^7 Hz.

Our conclusions are that the C3 furanose ring in the DNA sequence [d(CGC$_3$GAATTC$_9$GCG)]2 is puckering between two conformations, at a rate of 0.7×10^7 Hz, over a potential barrier of $5.5k_BT$ between the two conformations, and a puckering amplitude of 0.4 Å. We propose this exact set of parameters of C3 only as the furanose rings at different positions do not have identical experimental results. However, C9 has shown large amplitude motions on the order of 38°. We propose that other dynamic furanose rings could exhibit similar behavior as C3 and have similar energetics. These sites could have a different set of specific parameters, but the furanose ring could still be diffusing through a potential energy surface, rather than exhibiting activated exchange. The C9 line shape has a similar form[14] to the simulation in Figure 8b, with a puckering amplitude of 0.5 Å. We conclude that a diffusive model is an improvement over an activated exchange model for dynamic furanose rings.

The natural extension of this model is to include all members of a nucleotide subunit from one phosphate group to the next one, and determine whether inclusion of these substituents affects the sugar ring motion, and vice versa. Additionally, this can allow for investigation of the motion of other parts of the nucleotide, and how the dynamics propagate among them, and how they are correlated. This is currently being investigated.

Another interesting comparison of dynamical models is to compare the degree of maximum angular displacement. When there is a puckering amplitude of $q = 0.4$ Å, the maximum angular displacement is $\theta = 36°$. This compares to the angular displacement of $\theta = 38°$ for previous work using a two-site jump to model motionally averaged furanose ring line shapes.[14] Additionally, "rigid" line shapes that retain the Pake doublet form have been successfully simulated by using a two-site jump of small amplitude (∼10°) to replicate line shapes.[29,45] These are comparable to simulations using our new diffusive model with a puckering amplitude of $q = 0.2$ Å, which has a maximum angular displacement of $\theta = 19°$.

In addition to aiding in structural studies of nucleic acid conformation, the conclusions drawn may have a wider impact. It has been proposed previously that the amplitude of local DNA dynamics has a correlation to local helical flexibility.[27,49] Furanose rings that exhibit large amplitude motions are regions of increased local conformational flexibility. This increased conformational flexibility may indicate that the DNA is an active participant in protein−DNA interactions, where the increased local flexibility lowers the energy barrier necessary for protein−DNA binding,[27,49] again allowing for easier binding to the DNA. If the motion of the furanose rings can be effectively quantified, this information may go a long way toward identifying a role for the internal dynamics in DNA−protein interactions.

Acknowledgment. This research was supported by NIH grant RO1 GM58914-01. Gary Meints acknowledges the support from NIH Training Grant GM32681. The authors would like to thank Professors R. L. Vold and R. R. Vold for providing copies of MXET1.

JA010721D

(48) Edholm, O.; Blomberg, C. *Chem. Phys.* **1979**, *42*, 449−464.

(49) Meints, G. A. J.; Drobny, G. P. *Biochemistry*. Accepted for publication.